'This is the peer reviewed version of the following article: Ryan MK, Mohtar AA, Cleek TM, Reynolds KJ. Time-elapsed screw insertion with microCT imaging. Journal of Biomechanics. pii: S0021-9290(15)00727-7. doi: 10.1016/j.jbiomech.2015.12.021. Available online 18 December 2015.

which has been published in final form at

DOI:
http://dx.doi.org/10.1016/j.jbiomech.2015.12.021

Time-elapsed screw insertion with microCT imaging

Ryan, MK; Mohtar, AA; Cleek, TM; Reynolds, KJ

Keywords:

Time-elapsed, cancellous bone, insertion torque, screw insertion

Medical Device Research Institute,

School of Computer Science, Engineering and Mathematics

Flinders University

GPO Box 2100, Adelaide, South Australia, 5001 Australia

P: +618 8201 3363

E: melissa.ryan@flinders.edu.au

Abstract

Time-elapsed analysis of bone is an innovative technique that uses sequential image data to analyze bone mechanics under a given loading regime. This paper presents the development of a novel device capable of performing step-wise screw insertion into excised bone specimens, within the microCT environment, whilst simultaneously recording insertion torque, compression under the screw head and rotation angle. The system is computer controlled and screw insertion is performed in incremental steps of insertion torque. A series of screw insertion tests to failure were performed (n=21) to establish a relationship between the torque at head contact and stripping torque (R^2 = 0.89). The test-device was then used to perform step-wise screw insertion, stopping at intervals of 20%, 40%, 60% and 80% between screw head contact and screw stripping. Image data-sets were acquired at each of these time-points as well as at head contact and post-failure. Examination of the image data revealed the trabecular deformation as a result of increased insertion torque was restricted to within 1mm of the outer diameter of the screw thread. Minimal deformation occurred prior to the step between the 80% time-point and post-failure. The device presented has allowed, for the first time, visualization of the micro-mechanical response in the peri-implant bone with increased tightening torque. Further testing on more samples is expected to increase our understanding of the effects of increased tightening torque at the micro-structural level, and the failure mechanisms of trabeculae.

1 INTRODUCTION

Fracture fixation in osteoporotic bone is challenging due to a combination of reduced bone volume and microstructural changes (Giannoudis and Schneider, 2006). Over the next 50 years, the number of osteoporosis related fractures is expected to increase more than three-fold (Kanis, 2007), which highlights the need to increase our understanding of the factors that promote fracture consolidation and those that impede it.

Thomas et al. (2008) identified three major phases of screw placement (Figure 1); Firstly 'insertion', whereby a gradual rise in torque occurs as a result of the cumulative friction between the bone and the screw as increasingly more threads engage. In the case of a lag screw, once all threads have engaged a plateau in the torque occurs, due to only the leading thread cutting into the bone. This is followed by 'tightening', which occurs as the head of the screw comes into contact with the bone or plate. The threads of the screw are forced against the newly formed threads in the bone, resulting in an increased resistance to the applied torque, characterized by a steep increase in slope of the torque versus screw rotation trace. The final phase, 'stripping', shows a decrease in torque as the screw threads shear through the bone material (Figure 1). Previous work within our laboratory has established a strong relationship between the plateau insertion torque, measured at head contact (T_{HC}) and the maximum tightening torque (T_{max}) in bone surrogates, as well as excised ovine vertebral and human femoral head specimens (Reynolds et al., 2013), which presents the ability to predict T_{max} based solely on the torque required to achieve head contact.

"Time-elapsed analysis" of bone is an emerging technique using sequential image acquisition to analyse bone mechanics under a given loading regime. Nazarian and

Müller (2004) validated the use of this method to evaluate microstructural trabecular mechanics under uniaxial loading, demonstrating no difference in the macroscopic behaviour of cancellous bone specimens under continuous or step-wise loading conditions. To date, this procedure has been employed in combination with micro computed tomographic (microCT) imaging during uniaxial compression tests (Müller et al., 1998; Nazarian and Müller, 2004; Zwahlen et al., 2013, 2015), screw pull-out (Gabet et al., 2010), and screw push-in tests (Mueller et al., 2013) as well as in combination with synchrotron imaging (Thurner et al., 2006). These studies have provided valuable insight into the failure mechanisms of bone under specific loading conditions.

Work within our laboratory, however, has sought to better understand the interactions between bone and implant during screw placement. The purpose of this study was to develop a device and technique that would allow time-elapsed assessment of trabecular mechanics during the tightening phase of screw insertion. Specifically, the aim was to develop a system that would allow the acquisition of microCT images, at pre-defined percentages of stripping torque; allowing, for the first time, visualization of the deformation of the peri-implant trabeculae with increasing insertion torque.

The steps to achieve this aim were:

(1) Design a device that can operate within the microCT scanner capable of inserting screws into bone to preset levels of ultimate failure torque (as predicted by T_{HC});

(2) Undertake experimental screw insertion tests to failure to determine the relationship between T_{HC} and T_{max};

(3) Demonstrate the system's ability to stop at programmable pre-set levels of T_{max}, using the algorithm developed in (2) and in combination with sequential microCT image acquisition.

2 METHODS

2.1 Tissue Collection

Nine human femoral head samples (males = 5; females = 4) were collected from routine arthroplasty cases from patients who had suffered non-traumatic hip fractures, (Orthopaedics and Trauma department, Royal Adelaide Hospital, SA). Femoral heads were collected from donors, wrapped in saline soaked gauze, and stored fresh at -20°C until required. Average (S.D.) age of donors at time of collection was 75 (12) years. All donors of the specimens had given their consent for use in research and ethical approval was obtained from the local Human Research Ethics Committee.

2.2 Screws

Custom-manufactured, aluminium (Al) screws were produced, based on the geometry of a commercially available partially threaded lag screw (Catalog No. 7111-9106, Smith and Nephew, London UK). Screws had a thread length of 16mm, inner diameter (ID) of 5.2mm, outer diameter (OD) of 7.0mm and pitch of 2mm (Figure 2). Al was chosen due to its radiolucency and strength properties with respect to bone tissue.

2.3 Test-Rig

To allow visualization of the bone-implant interface, a custom-designed, computer controlled test rig was created to fit inside the Skyscan live animal 1072 µCT scanner (Figure 3). The housing of the test-rig was fabricated from Al to minimize artefact during image acquisition. The device comprises a polymer base plate to which the specimen is attached, a 1.1kN compression load cell (Model Number: THB-250S, Transducer Techniques, CA, USA) that sits under the screw head, an 11Nm torque transducer (Model number: TRT-100, Transducer Techniques, CA, USA), an A-max 20W motor with graphite brushes (Model number: 23667, Maxon motor AG, Switzerland), coupled with a ceramic planetary gearhead (Model number: 166952, Maxon motor AG, Switzerland) and a 500 counts-per-turn rotary encoder (Model number: 110513, Maxon motor AG, Switzerland). Coupling the gear-system with the torque transducer, the entire system was calibrated in a NATA certified laboratory and is capable of measurements up to 12 Nm with an accuracy of ±0.2 % and loads of 450 N with an accuracy of ±0.64 N.

The test-rig is computer-controlled using custom written software (Labview, V8.2, National Instruments Corporation, Austin, Tx, USA). The device operates in two modes; “position control”, or “torque control”. In “position control”, the rotation angle is input by the user, and the screw is rotated until the desired rotation is achieved. In “torque control” the screw is firstly tightened until “head contact” is achieved, where head contact is defined by a user set threshold detected by the compression transducer. Once head contact is achieved, the system calculates T_{HC} by averaging the torque trace over the 60 degrees of rotation preceding head contact. The value of T_{HC} is then used to predict

T_{max} using the algorithm developed in section 2.5. Finally, the test-rig will perform time-elapsed insertions to predefined percentage levels of [(T_{max} – T_{HC}) + T_{HC}].

2.4 Specimen Preparation

The lateral face of all femoral heads were sectioned using a surgical hand saw to ensure a smooth surface for gluing and a minimum specimen height of 35mm, to provide sufficient depth and access for screw placement. Specimens were prepared whilst frozen and immediately returned to the freezer.

Specimens were thawed at 3°C overnight prior to insertion. Excess moisture was removed from the specimen face using paper towels, and the face was then sanded and wiped with alcohol.

The insertion points for screw placement were chosen based on the inverted triangle used clinically for fixation of femoral neck fractures using cancellous bone screws (Figure 4) (Selvan et al., 2004). Hole 1 was created in the anterior superior aspect of the femoral head, hole 2 in the posterior superior aspect, and hole 3 in the central inferior aspect.

In some specimens, a surgical extraction hole was present in the femoral head. If visual inspection of specimens revealed extraction holes were evident within 5 mm of the screw insertion site, no screw was inserted into the hole location for that specimen. Wirth et al. (2011) have demonstrated that the average effective strain is reduced by 90% at distances greater than 5mm from the outer thread, so regions outside of this were deemed suitable for screw insertion. Depending on the presence and location of the extraction hole, between one and three insertions were made, ensuring any extraction hole did not impact screw placement.

Specimens were glued to the base plate using cyanoacrylate and clamped for 15 minutes to ensure a strong bond. Once specimens were attached, the base-plate was clamped in a vice for drilling.

For each screw insertion, a 5.2mm pilot hole was drilled to a depth of 35mm using a table top drill press (ZQJ-4116, Ledacraft, Aus). Without removing the bone from the drill press, a stainless steel washer and the load cell were inserted under the screw head, and the screw was inserted by manually rotating the chuck of the drill press until approximately 15mm of clearance between the screw head and washer remained. The bone-screw construct was then transferred to the test-rig for either continuous or step-wise insertion.

2.5 Continuous Screw Insertion to Failure

The remaining screw insertion was performed automatically by the test-rig using the "position control" mode. The position was set to 5400 degrees (i.e. 15 full revolutions), which would ensure that the screw would fully insert and strip. The screws were inserted at a rate of 5 revolutions per minute (rpm), whilst insertion torque and compression under the head of the screw were simultaneously recorded at a sample rate of 20Hz. All screws were inserted continually until failure occurred. Screws were used three times before a new screw was implemented.

The torque and compression traces were analysed using a custom program (Matlab, MA, USA). The point of head contact was defined as the point where the slope of the compression trace exceeded a threshold level of 10 N/deg. This value was chosen as the smallest value obtained by incrementally varying the slope threshold until head contact was appropriately defined for all tests; using a lower value for the threshold resulted in the software incorrectly detecting head contact too early for some specimens. This threshold was selected as it most reliably detected head contact for all specimens. T_{HC} was determined by averaging the torque trace over the 60° preceding head contact. Stripping torque was defined as the maximum torque measured by the torque transducer (T_{max}). The maximum compressive force (C_{max}) was defined as the maximum force measured by the load cell.

2.6 Time-elapsed Screw Insertion

To perform time-elapsed screw insertion, one specimen was tested. The specimen was prepared according to the same methods described in section 2.4; however before drilling the hole, the specimen underwent microCT imaging and the first dataset was obtained (Dataset 1 = “Pre-Drill”). The specimen was removed from the scanner and the screw was inserted according to the methods described in section 2.4. The system was then placed inside the microCT scanner and the screw was tightened to head contact using the test-rig in “torque control” mode. Once the system detected head contact, it was programmed to automatically cease insertion, and a microCT dataset was obtained (Dataset 2 = “Head Contact”).

The continuous screw insertion analysis used a threshold of 10N/deg on the slope of the compression trace for identifying head contact; however implementing this in real time is challenging; consequently a single-value compression threshold of 2N, measured by the compression transducer, was used to detect head contact. This value was chosen, as the lowest value that would detect a load by the compression transducer, without early detection due to noise in the signal.

The value of T_{HC} determined by the test rig was used to predict the torque at which the screw would strip the bone threads. Based on this prediction, the device was programmed to stop at 20%, 40%, 60%, 80% and 100% of predicted $[(T_{max} – T_{HC}) + T_{HC}]$ (Figure 1). At each of these torque intervals, a microCT image dataset was acquired (Dataset 3 = "20% image", Dataset 4 = "40% image", etc). Screw insertion was programmed to stop automatically if the desired torque level was not achieved within 360° of rotation.

To validate the step-wise test method a further 10 step-wise screw-insertion tests were performed as described above. The insertion traces were analysed to extract the T_{HC} and T_{max} and the relationship between the two variables for the continuous and step-wise insertion methods was compared.

2.6.1 Micro Computed Tomographic Imaging (microCT)

Each of the image datasets (Pre-drill, Head Contact, 20% image, etc) was obtained using the SkyScan 1072 microCT scanner. Images were acquired at an isotropic resolution of 17.4µm/pixel, operating at 100kv, 80µA, with a 1mm Al filter, two frame averaging and a step size of 0.5˚. Bitmap images were obtained by cone-beam reconstruction (NRecon, SkyScan). After reconstruction, images were registered to the "Head-contact" scan, using the 3D registration module in DataViewer (v1.5.1.2, Bruker, Kontich, Belgium), which applies rigid transformations (translations along x,y and z, and rotations about x, y and z) to the target image and attempts to minimise the sum of squared differences as the correlation criteria.

The registered images were coarsened to 60μm and noise was reduced using a three-dimensional Gaussian filter with a radius of 1 voxel.

A global threshold was implemented to isolate the screw geometry (grey values greater than 190 were considered screw). An erosion cycle of 1 pixel was then performed followed by four cycles of dilation (radius = 1 pixel). The erosion was performed to eliminate spicules on the screw surface due to image artefact. The dilation cycles increased the actual diameter of the screw, but were necessary to eliminate debris at the bone-screw interface that appeared as structurally intact bone during the segmentation of the bone. This resulted in a 360μm thick increase in screw OD. The bone was segmented by implementing Otsu's automatic threshold technique in three-dimensions and the screw geometry was then subtracted from this (CTAn, v1.10.11). Segmented volumes for each dataset were calculated using ScanIP (Simpleware, Devon, UK), the software counts each voxel that has been classified as either bone or screw and uses the voxel resolution to provide a volumetric measure of bone and screw. These volumes were compared between time points, to ensure segmentation techniques maintained consistent overall volumes for both bone and screw between time points.

2.7 Statistical Analysis

Shapiro-Wilks tests showed torque data (T_{HC} and T_{max}) were normally distributed. Mean and standard deviation (SD) of measured variables are reported in Table 1. Linear regression analysis was conducted to determine the relationship between T_{HC} and T_{max}.

Student's t-tests were used to compare segmented volumes of bone and screw between time points and to compare the slope and intercept values for the regression traces for the two insertion methods. Fisher's z-transform was used to compare the correlation coefficient for the two insertion methods. All statistical analysis was performed in SPSS (v20, SPSS, Inc, Chicago, Il) with $p < 0.05$ considered significant.

3 Results

3.1 Continuous Screw Insertion

Twenty-one continuous insertion tests to failure were conducted into eight specimens. The mean (SD) T_{HC} and T_{max} were 1.05Nm (0.54) and 2.33Nm (0.89), respectively. The average C_{max} was 766 N (307) (Table 1). On average (SD), T_{HC} equated to 43.2% (7.8) of T_{max}. A strong linear relationship was observed between T_{HC} and T_{max} (R^2 = 0.90, $p <$ 0.001) (**Error! Reference source not found.**) with a standard error of 0.27Nm. The average (SD) rotation angle between T_{HC} and T_{max} was 107° (33°).

3.2 Time-elapsed screw insertion

Fisher's z-transform showed no difference in the strength of the relationship between the two insertion method (p=0.53). Student's t-tests revealed no difference in the slope (p=0.98) or the y-intercept (p=0.48) for the two regression lines for T_{HC} and T_{max} (**Error! Reference source not found.**), confirming the step-wise insertion method did not influence the resultant stripping torque.

A single femoral head was used to analyse the efficacy of the system for time-elapsed screw insertion. The software calculated T_{HC} to be 1.43Nm; implementing the algorithm determined from the continuous insertion tests, the software predicted that the screw would strip at 2.93 Nm and the motor was programmed to stop at 1.72Nm, 2.02Nm, 2.33Nm, 2.63Nm and 2.93Nm, representing 20%, 40%, 60%, 80% and 100% of (2.93Nm – 1.43Nm). Actual stripping torque occurred at 2.92Nm and consequently the motor did not stop at the 100% failure point. This was noted on the live torque trace (by a decreasing slope) and the motor was manually stopped 46° past failure and a "post-failure" image was taken.

The predicted and actual torque levels and the resultant torque and compression versus degrees of rotation trace are shown in

Table 2 and **Error! Reference source not found.**, respectively. The spikes observed in each of the traces occur at the points where the motor was stopped and an image dataset was acquired. When the motor stops for image acquisition, the motor is switched off to ensure it does not interfere with scanning. Consequently, a downward spike in the torque trace occurs. After scanning, the motor switches back on and insertion continues; this causes a sharp positive spike in the torque trace, which is due to the system overcoming the static friction to continue rotation and motor control system's limitation to react to the rapid torque change. The torque trace then continues along the original insertion slope.

Smoothing was performed using a moving average filter to remove spikes and retain the overall shape of the compression and torque traces. Initially a moving average filter (window = 60) was applied over the region containing the spikes in the torque trace. The entire torque trace and then compression trace then underwent a moving average filter with a smaller window (window = 20). T_{HC}, T_{max} and C_{max} were: 1.49Nm, 2.92Nm, and 979N respectively.

Image datasets were successfully obtained at pre-drill, head-contact, and the 20%, 60%, 80% and post-failure time points. The image data set obtained at the 40% time-point was corrupted and unable to be analysed, however this was due to the image acquisition software and did not affect the screw insertion.

The mask volumes at each time point are shown in

Table 3, demonstrating the segmentation techniques maintained consistent overall volumes between time points. To visualize the trabecular deformations, 3D slices are shown in Figure 7, demonstrating significant deformation is only observed in the post-failure step.

4 Discussion

Fracture fixation in osteoporotic bone is challenging due to both degradation in bone quality as well as reduced bone stock. In the case of a lag screw, stability is achieved by bone contact and inter-fragmental compression; however there is no empirical evidence to suggest what level of compression (and consequently insertion torque) is ideal for primary bone healing. Clinically, insertion torque is the only measure the surgeon has, to determine if a stable fixation has been achieved. Higher insertion torques reportedly result in greater compression (Ricci et al., 2010), however in trying to achieve this, screw stripping during insertion occurs with an incidence as high as 45% (Stoesz et al., 2014).

The main goal of this study was therefore to design a device capable of performing screw insertion tests, to predefined levels of $T_{max,}$ within a microCT scanner, in conjunction with time-elapsed image acquisition to evaluate the effects of increased tightening torque on micro-scale behavior. The test-rig devised herein allows for the first time, the measurement of compression, insertion torque as well as visualization of the bone-implant interface during the tightening and stripping phases of screw insertion. No difference was observed in the torque versus angular rotation traces between the insertion methods (Figure 5). This is consistent with the results observed by Nazarian and Müller (2004), who demonstrated no difference in stress-strain curves for whale and human vertebral bone under either step-wise or continuous uniaxial loading. This demonstrates that the step-wise method of screw insertion devised herein is a valid technique to analyse the interactions between bone and screw at the micro-structural level.

For screw insertion, an aluminium screw was used over commercially available stainless steel (SS) or titanium (Ti) due to the known effects of metal in microCT scanners (Lee et al., 2007). A series of tests to failure (n = 21), were conducted to establish the unique relationship between T_{HC} and T_{max} for the specific screw under consideration. Based on these, a strong linear relationship between T_{HC} and the T_{max} was observed ($R^2 = 0.90$, $p < 0.001$). The differences in the observed regression slopes between this study and the study by Reynolds et al. (2013) are likely due to the difference in bone quality; the latter study considered a combination of osteoporotic and osteoarthritic bone specimens, whereas this study looked specifically at only specimens retrieved from patients that had experienced a non-traumatic hip fracture. Consequently, the bone from this study was of a poorer quality, which likely contributed to the smaller regression slope.

On average T_{HC} equated to 47% of T_{max}, and the average (SD) rotation angle between head contact and stripping equated to 107° (33). The doubling of the torque over such a small rotation angle highlights the precision required of the surgeon to ensure stability, without over tightening.

For the time elapsed screw insertion, the device was able to predict T_{max} and stop at the pre-defined time-points between head contact and stripping. The error between predicted stopping torque and measured torque for each of the time points was largest for the 20 % and 40 % steps and decreased as the torque approached T_{max} (Table 2). The smaller error with increasing torque could be attributed to an increase in signal-to-noise ratio (SNR) with increasing torque, however this is only a single specimen. The correlation observed in the continuous insertion data (Fig 5) demonstrates that T_{max} is not completely predicted by T_{HC} and under or over estimations of T_{max} are likely. In this test, the predicted stripping torque was 2.93Nm, and the recorded T_{max} was 2.92Nm (0.3 %). Since the predicted torque was greater than the actual T_{max} the system did not stop at stripping and a post-failure image was acquired instead.

Image datasets were successfully obtained at ‘pre-drilling’, ‘head contact’ and the 20, 60 and 80% time-points as well as ‘post-failure’. The segmented volumes of bone and screw are listed in Table 3 and show the change in bone volume from the head contact data set was less than 5%. The largest discrepancy was for the failure scan and is most likely due to the substantial volume of debris generated as the threads shear through the bone. The screw volume remained consistent throughout scans.

Examination of the time-elapsed image data showed little deformation occurred in the peri-implant trabeculae prior to the step between 80% [(T_{max} – T_{HC}) + T_{HC}] and post failure, suggesting that tightening to levels above 80% [(T_{max} – T_{HC}) + T_{HC}] may put the stability of the bone-screw construct at risk; but before this, the effects on the local trabecular network appear minimal. Visual inspection suggests trabecular deformation was restricted to within the screw threads, with the rest of the bone remained relatively unaffected (**Error! Reference source not found.**). Wirth et al. (2011) also noted normalized average effective strain was negligible outside a distance of 5 mm from the outer thread, for a cancellous bone screw with an outer diameter of 3.5 mm and pitch of 1 mm, suggesting the majority of damage is restricted to a small radius around the screw OD. Quantification of induced bone-strains would likely extend outside the peri-implant bone, but it is expected that this would be restricted to within a few millimeters of the screw thread OD. The time-elapsed data allows, for the first time, the ability to track the movement of individual trabeculae with increasing screw tightening (**Error! Reference source not found.**). The fact that little deformation was evident until the post-failure data set suggests that the majority of deformation leading to overall failure occurs post apparent yield torque. To date we have not characterized the localized failure mechanisms leading to screw stripping, however the device described herein provides a significant step towards this.

It is important to note the limitations of this study; firstly Al screws were used, to enable visualization of the bone-screw interface. Future studies may consider the use of ceramic or PEEK screws, which are radiopaque, however the strength characteristics with respect to femoral head bone would need to be considered. A further limitation was the debris induced around the screw as a consequence of insertion. This remains in direct contact with the screw and when segmenting the bone and screw, appears as structurally intact bone. This results in a larger volume of bone in contact with the screw, which in reality most likely does not provide any structural support. Trying to differentiate the debris from the structurally intact bone was not addressed herein, but is an important consideration in future work. Although not common practice clinically in osteoporotic bone, tapping of the thread prior to screw placement would be beneficial in removal of debris. Furthermore, these results have only been reported for a single, excised specimen from one anatomical location. The absolute torque and compression may vary when screws are inserted clinically and into bone from different locations. The effects of creep have not been considered in this work. Common clinical practice is for the surgeon to tighten screws, allow stress relaxation to take place and to then administer a final tightening. Stress relaxation is an important consideration, and we noted a small amount of relaxation occurred in both the torque and compression traces during image acquisition. The effects of this will be addressed in future work. Finally, these data are reported for “time-zero” (i.e. at the time of screw insertion) and are in absence of any remodeling; longitudinal analysis of screw stability would also need to be considered to enable further inferences with respect to “optimal” tightening levels.

Whilst maximum achievable compression is desirable, this needs to be considered in light of the concomitant damage induced in the peri-implant bone with increased application of torque, and the subsequent risk of screw stripping. If sufficient compression can be achieved that can provide adequate fracture stability, with lower applied torque, then the need to attain torques close to stripping may be reduced.

Although the device presented here does not offer any direct clinical application, its usefulness lies in the ability to conduct a thorough investigation of the effects on the bone in contact with the screw at the micro-structural level, as a function of increasing torque. This may have clinically implications, in light of recent literature that has demonstrated the strong relationship between T_{HC} and T_{max} (Reynolds et al., 2013). Further testing on additional specimens and alternate screw designs will provide information regarding the failure mechanisms of the peri-implant bone during tightening. In conjunction with digital volume correlation (DVC) or finite element analysis, this will allow quantification of the peri-implant bone strains generated during screw tightening which will allow characterisation of the failure modes of the peri-implant bone. Ultimately this may lead to superior screw design or insertion technique.

In conclusion, the novel device presented herein has allowed, for the first time, visualization of the induced trabecular deformation in response to applied insertion torque after head contact. The applications of this to further specimens will allow qualitative and, in combination with FEA or digital volume correlation, quantitative information to relate applied torque to the induced mechanics of the peri-implant bone. How these responses (e.g. modes of failure and levels at which failure occurs) may differ with different screw geometries and materials may have future clinical implications, particularly in the design of hardware and techniques of insertion for fracture fixation of osteoporotic bone.

CONFLICT OF INTEREST

All authors declare there are no conflicts of interest with regard to the carrying out and reporting of this research.

FUNDING

This research was supported by a grant from the National Health and Medical Research Council, Grant ID 595933.

ACKNOWLEDGMENT

The authors kindly thank Richard Stanley for his invaluable contributions in the biomechanical testing of this study.

REFERENCES

Gabet, Y., Kohavi, D., Voide, R., Mueller, T., Muller, R., Bab, I., 2010. Endosseous implant anchorage is critically dependent on mechanostructural determinants of per-implant bone trabeculae. Journal of bone and mineral research 25, 575-583.

Giannoudis, P., Schneider, E., 2006. Principles of fixation of osteoporotic fractures. The Journal of Bone and Joint Surgery 88-B, 1272-1278.

Kanis, J., 2007. Assessment of osteoporosis at the primary health care level, in: Group, W.S. (Ed.), University of Sheffield, UK.

Lee, M.J., Kim, S., Lee, S.A., Song, H.T., Huh, Y.M., Kim, D.H., Han, S.H., Suh, J.S., 2007. Overcoming artifacts from metallic orthopedic implants at high-field-strength MR imaging and multi-detector CT. Radiographics 27, 791-803.

Mueller, T., Basler, S., Muller, R., Van Lenthe, G., 2013. Time-lapsed imaging of implant fixation failure in human femoral heads. Medical Engineering & Physics 35, 636-643.

Müller, R., Gerber, S., Hayes, W., 1998. Micro-compression: a novel technique for the nondestructive assessment of local bone failure. Technology and Health Care 6, 433-444.

Nazarian, A., Müller, R., 2004. Time-lapsed microstructural imaging of bone failure behavior. J Biomech 37, 55-65.

Reynolds, K., Cleek, T., Mohtar, A., Hearn, T., 2013. Predicting cancellous bone failure during screw insertion. Journal of biomechanics 46, 1207-1210.

Ricci, W., Tornetta, P.r., Petteys, T., Gerlach, D., Cartner, J., Walker, Z., Russell, T., 2010. A comparison of screw insertion torque and pullout strength. Journal of orthopaedic trauma 24, 374-378.

Selvan, V., Oakley, M., Rangan, A., Al-Lami, M., 2004. Optimum configuration of cannulated hip screws for the fixation of intracapsular hip fractures: a biomechanical study. Injury 35, 136-141.

Stoesz, M., Gustafson, P., Bipinchandra, V., Jastifer, J., Chess, J., 2014. Surgeon perception of cancellous screw fixation. Journal of orthopaedic trauma 28, e1-e7.

Thomas, R., Bouazza-Marouf, K., Taylor, G., 2008. Automated surgical screwdriver: Automated screw placement. Proceedings of the institution of mechanical engineers 22, 451-454.

Thurner, P., Wyss, P., Voide, R., Stauber, M., Stampanoni, M., Sennhauser, U., Muller, R., 2006. Time-lapsed investigation of three-dimensional failure and damage accumulation in trabecular bone using synchrotron light. Bone 39, 289-299.

Wirth, A.J., Goldhahn, J., Flaig, C., Arbenz, P., Muller, R., van Lenthe, G.H., 2011. Implant stability is affected by local bone microstructural quality. Bone 49, 473-478.

Zwahlen, A., Christen, D., Ruffoni, D., Schneider, P., Schmolz, W., Muller, R., 2013. Image-guided failure assessment of human trabecular bone - Inverse finite element modelling for characterization of elastic properties. Biomedizinische Technik. Biomedical engineering.

Zwahlen, A., Christen, D., Ruffoni, D., Schneider, P., Schmolz, W., Muller, R., 2015. Inverse Finite Element Modeling for Characterization of Local Elastic Properties in Image-Guided Failure Assessment of Human Trabecular Bone. Journal of biomechanical engineering 137.

Figures

Figure 1: Torque versus rotation angle during screw insertion of a lag screw into human cancellous bone. Three distinct regions are identifiable: Insertion is defined as the region prior to head contact, the slope of the trace continues to increase as more and more threads are engaged; tightening occurs after head contact and is characterised by the steep increase in slope; the final phase (stripping) occurs once T_{max} is achieved and the slope of the trace becomes negative. The test-rig has been designed so that step-wise screw insertion can be performed utilising an algorithm developed to predict T_{max} based on T_{HC}.

MicroCT image data is acquired at the time-points indicated on the above graph, allowing time-elapsed assessment of the micro-scale interactions between bone and screw with increasing insertion torque.

Figure 2: Aluminium screw employed. The screw was custom manufactured from high grade aluminium; the geometry was based on a commercially available partially threaded cancellous lag screw from Smith and Nephew (Catalog No. 7111-9106, Smith and Nephew, London UK).

Figure 3: Custom designed test rig. Schematic (top) and actual device (bottom). The test rig comprises a 1.1 kN load cell and 11 Nm torque transducer, 20W motor, encoder and polymer base plate. The rig is computer controlled with custom developed software. Both torque and compression under the head of the screw are simultaneously recorded at 25kHz during screw tightening.

Figure 4: Excised femoral head indicating the location of the holes used for screw insertion. Hole 1 was created in the anterior superior aspect of the femoral head, hole 2 in the posterior superior aspect and hole 3 in the central inferior aspect.

Figure 5: Linear regression plot relating stripping torque (T_{max}) to the torque measured at head contact (T_{HC}) for aluminium cancellous bone screws inserted into excised femoral heads. T_{HC}, was defined as the average torque over 60° of rotation prior to head contact, T_{max} was defined as the maximum measured torque during insertion. The screws were

inserted either continuously or step-wise in combination with micro-CT imaging. No difference in the linear regression was observed between the two insertion methods.

Figure 6: Torque and compression versus rotations for the time-elapsed screw insertion into an excised human femoral head specimen. The spikes in the trace demonstrate the points where the motor was stopped to acquire image data sets. The bold lines represent the smoothed trace, which was used for the analysis. Smoothing was performed by a moving average filter.

Figure 6: 3D rendering depicting the deformation observed in the trabecular network surrounding the screw thread. The images were taken at head contact (top left), 20% $[(T_{max} – T_{HC}) + T_{HC}]$ (top middle), 60% $[(T_{max} – T_{HC}) + T_{HC}]$ (top right), 80% $[(T_{max} – T_{HC}) + T_{HC}]$ (bottom left), and post failure (bottom right). Deformation of individual spicules has been highlighted in colour: Orange and green illustrate crushing of a spicule on either side of the screw thread, pink illustrates a combination of bending and compression against a nearby spicule, and complete perforation of the spicule is shown in blue.

Tables

Table 1: Mean (SD) of the insertion parameters measured for the tests performed to failure (n=21).

Table 2: Comparison of the algorithm predicted and actual torque levels for time-elapsed screw insertion. The software reported T_{HC} as 1.43 Nm, and predicted T_{max} as 2.93 Nm. Actual stripping torque occurred at 2.92 Nm.

Table 3: Bone and screw volumes for the time-elapsed image data.

Figures

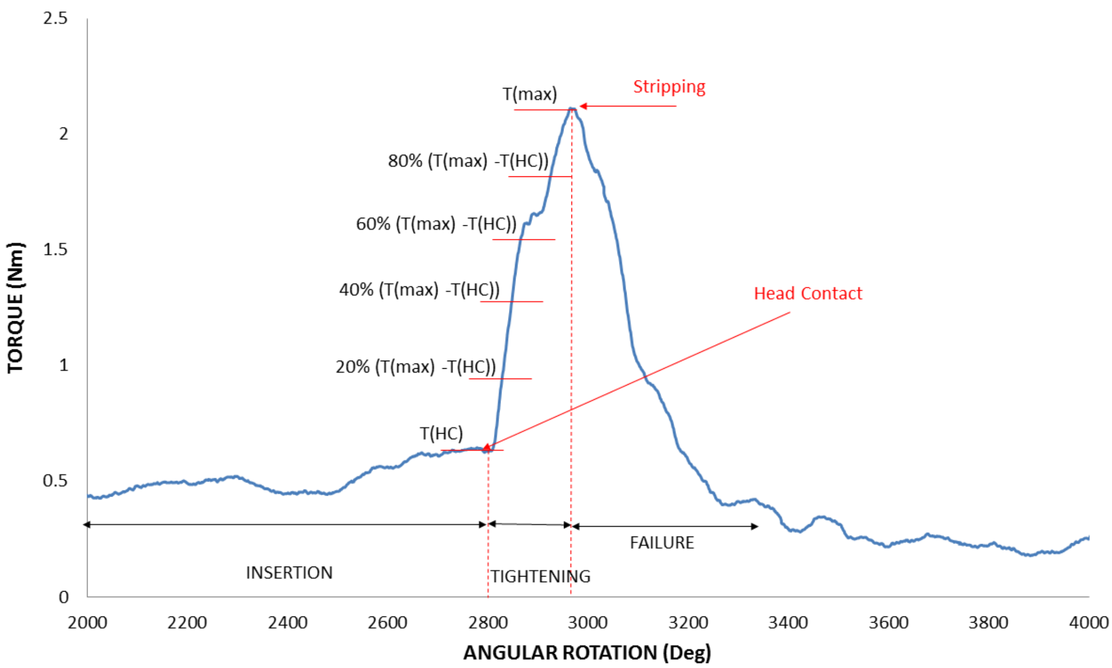

Figure 1: Torque versus rotation angle during screw insertion of a lag screw into human cancellous bone. Three distinct regions are identifiable: Insertion is defined as the region prior to head contact, the slope of the trace continues to increase as more and more threads are engaged; tightening occurs after head contact and is characterised by the steep increase in slope; the final phase (stripping) occurs once T_{max} is achieved and the slope of the trace becomes negative. The test-rig has been designed so that step-wise screw insertion can be performed utilising an algorithm developed to predict T_{max} based on T_{HC}. MicroCT image data is acquired at the time-points indicated on the above graph, allowing time-elapsed assessment of the micro-scale interactions between bone and screw with increasing insertion torque.

Figure 2: Aluminium screw employed. The screw was custom manufactured from high grade aluminium; the geometry was based on a commercially available partially threaded cancellous lag screw from Smith and Nephew (Catalog No. 7111-9106, Smith and Nephew, London UK).

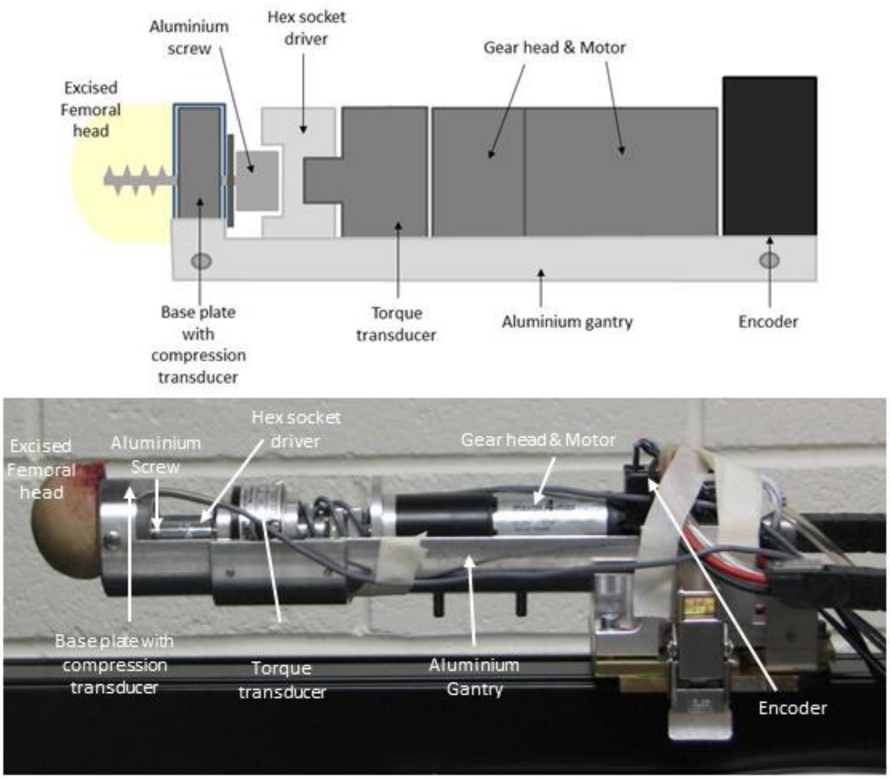

Figure 3: Custom designed test rig. Schematic (top) and actual device (bottom). The test rig comprises a 1.1 kN load cell and 11 Nm torque transducer, 20W motor, encoder and polymer base plate. The rig is computer controlled with custom developed software. Both torque and compression under the head of the screw are simultaneously recorded at 25kHz during screw tightening.

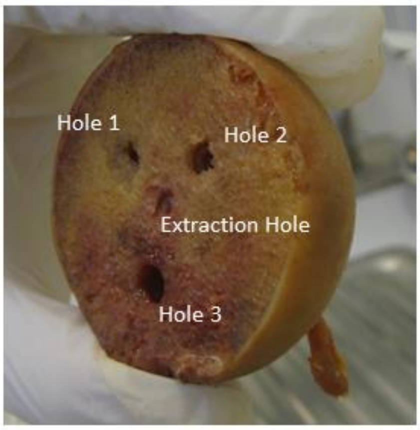

Figure 4: Excised femoral head indicating the location of the holes used for screw insertion. Hole 1 was created in the anterior superior aspect of the femoral head, hole 2 in the posterior superior aspect and hole 3 in the central inferior aspect.

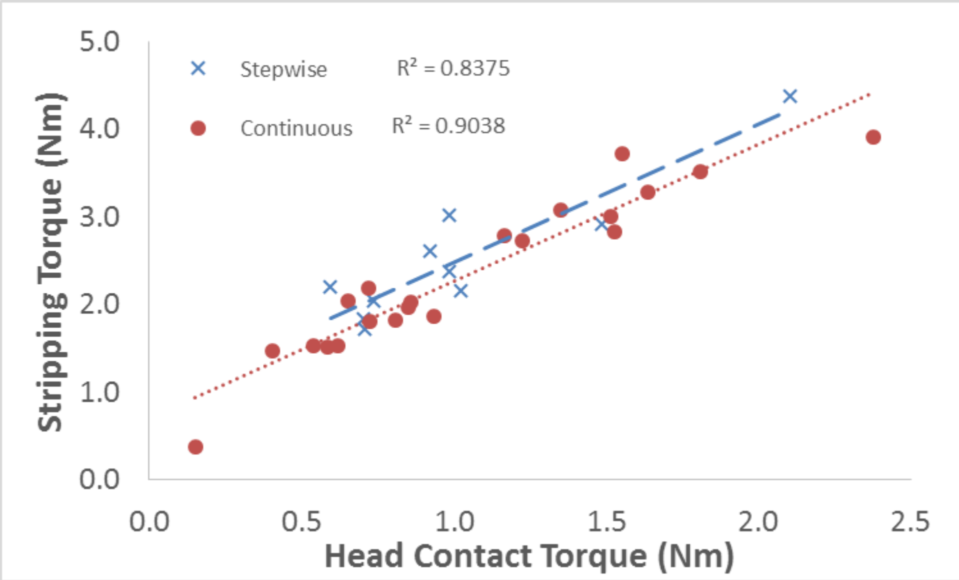

Figure 5: Linear regression plot relating stripping torque (T_{max}) to the torque measured at head contact (T_{HC}) for aluminium cancellous bone screws inserted into excised femoral heads. T_{HC}, was defined as the average torque over 60° of rotation prior to head contact, T_{max} was defined as the maximum measured torque during insertion. The screws were inserted either continuously or step-wise in combination with micro-CT imaging. No difference in the linear regression was observed between the two insertion methods.

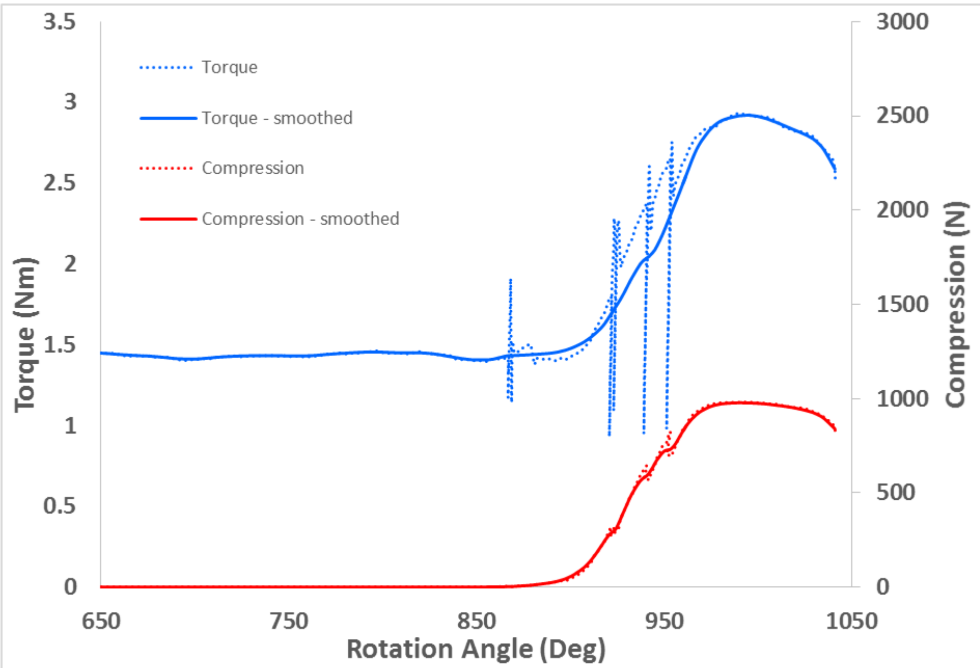

Figure 6: Torque and compression versus rotations for the time-elapsed screw insertion into an excised human femoral head specimen. The spikes in the trace demonstrate the points where the motor was stopped to acquire image data sets. The bold lines represent the smoothed trace, which was used for the analysis. Smoothing was performed by a moving average filter.

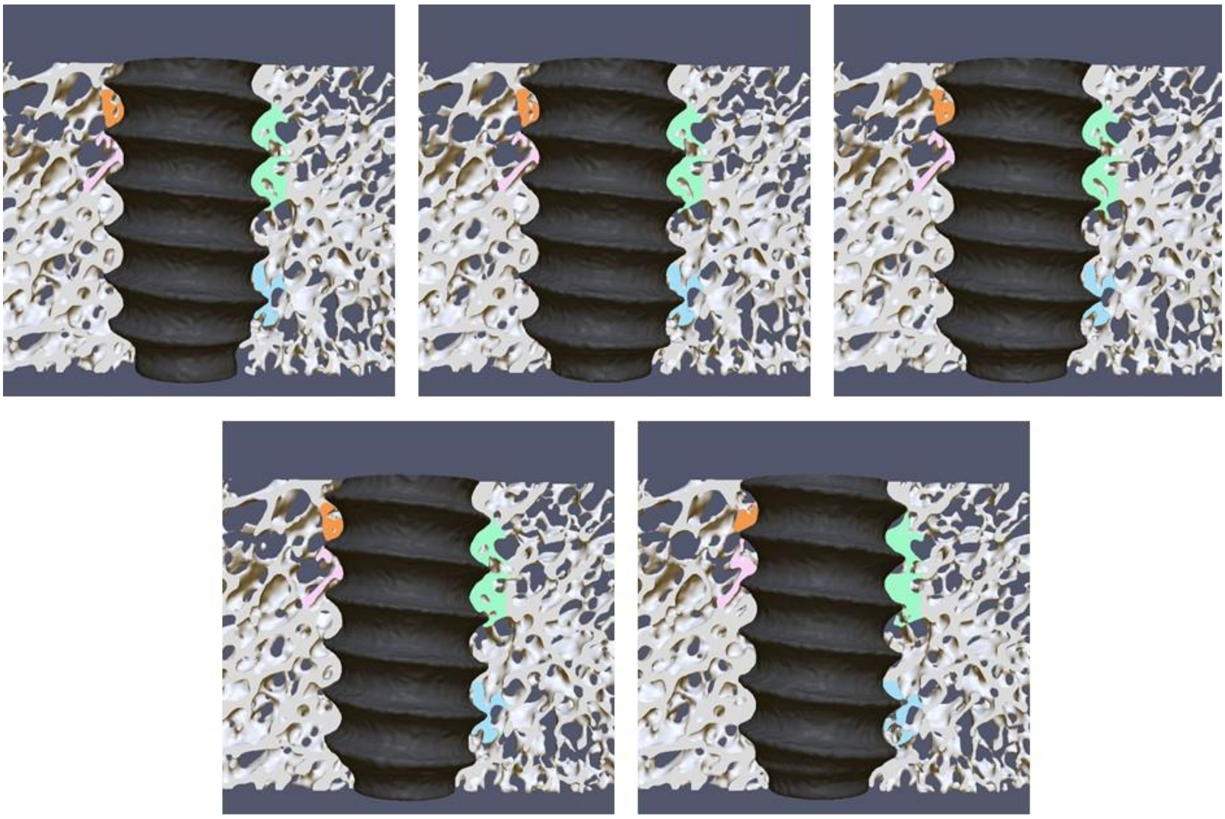

Figure 7: 3D rendering of a slice through the surrounding bone, depicting the deformation observed in the trabecular network surrounding the screw thread.The images were taken at head contact (top left), 20% [(T_{max} – T_{HC}) + T_{HC}] (top middle), 60% [(T_{max} – T_{HC}) + T_{HC}] (top right), 80% [(T_{max} – T_{HC}) + T_{HC}] (bottom left), and post failure (bottom right). Deformation of individual spicules has been highlighted in colour: Orange and green illustrate crushing of a spicule on either side of the screw thread, pink illustrates a combination of bending and compression against a nearby spicule, and complete perforation of the spicule is shown in blue.